JACS
JOURNAL OF THE AMERICAN CHEMICAL SOCIETY
Article
pubs.acs.org/JACS

# Fast Proton-Coupled Electron Transfer Observed for a High-Fidelity Structural and Functional [2Fe−2S] Rieske Model

Antonia Albers,[†] Serhiy Demeshko,[†] Sebastian Dechert,[†] Caroline T. Saouma,[‡,§] James M. Mayer,[‡] and Franc Meyer*[,†]

[†]Institute of Inorganic Chemistry, Georg-August-University Göttingen, Tammannstrasse 4, D-37077 Göttingen, Germany
[‡]Department of Chemistry, University of Washington, Box 351700, Seattle, Washington 98195-1700, United States

Supporting Information

**ABSTRACT:** Rieske cofactors have a [2Fe−2S] cluster with unique {$His_2Cys_2$} ligation and distinct Fe subsites. The histidine ligands are functionally relevant, since they allow for coupling of electron and proton transfer (PCET) during quinol oxidation in respiratory and photosynthetic ET chains. Here we present the highest fidelity synthetic analogue for the Rieske [2Fe−2S] cluster reported so far. This synthetic analogue $\mathbf{5}^{x-}$ emulates the heteroleptic {$His_2Cys_2$} ligation of the [2Fe−2S] core, and it also serves as a functional model that undergoes fast concerted proton and electron transfer (CPET) upon reaction of the mixed-valent (ferrous/ferric) protonated $\mathbf{5H}^{2-}$ with TEMPO. The thermodynamics of the PCET square scheme for $\mathbf{5}^{x-}$ have been determined, and three species (diferric $\mathbf{5}^{2-}$, protonated diferric $\mathbf{5H}^{-}$, and mixed-valent $\mathbf{5}^{3-}$) have been characterized by X-ray diffraction. p$K_a$ values for $\mathbf{5H}^{-}$ and $\mathbf{5H}^{2-}$ differ by about 4 units, and the reduction potential of $\mathbf{5H}^{-}$ is shifted anodically by about +230 mV compared to that of $\mathbf{5}^{2-}$. While the N−H bond dissociation free energy of $\mathbf{5H}^{2-}$ (60.2 ± 0.5 kcal mol$^{-1}$) and the free energy, $\Delta G^{\circ}_{CPET}$, of its reaction with TEMPO (−6.3 kcal mol$^{-1}$) are similar to values recently reported for a homoleptic {$N_2$/$N_2$}-coordinated [2Fe−2S] cluster, CPET is significantly faster for $\mathbf{5H}^{2-}$ with biomimetic {$N_2/S_2$} ligation ($k$ = (9.5 ± 1.2) × 10$^4$ M$^{-1}$ s$^{-1}$, $\Delta H^{\ddagger}$ = 8.7 ± 1.0 kJ mol$^{-1}$, $\Delta S^{\ddagger}$ = −120 ± 40 J mol$^{-1}$ K$^{-1}$, and $\Delta G^{\ddagger}$ = 43.8 ± 0.3 kJ mol$^{-1}$ at 293 K). These parameters, and the comparison with homoleptic analogues, provide important information and new perspectives for the mechanistic understanding of the biological Rieske cofactor.

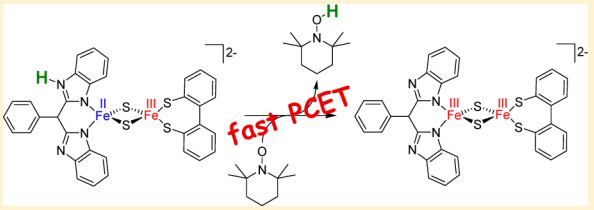


## INTRODUCTION

Rieske-type [2Fe−2S] clusters are unique biological electron transfer (ET) cofactors that feature a heteroleptic ligand environment distinct from that of common [2Fe−2S] ferredoxins, with one of the Fe atoms ligated by two cysteine thiolates and the other by two histidine imidazoles.[1] Rieske clusters serve as structural gates in bacterial oxygenase enzymes that catalyze oxidative hydroxylation of aromatic compounds, and they play an important role in the bifurcated Q-cycle of the quinol-oxidizing cytochrome complexes in respiratory and photosynthetic ET chains.[2,3] Histidine ligation is functionally relevant, since it enables coupling of electron and proton transfer upon reaction of the diferric Rieske cluster with hydroquinone substrates, producing the mixed-valent cluster that is protonated at the His ligands.[3,4] Redox potentials of Rieske [2Fe−2S] clusters in *bc*-type proteins have indeed been found to be pH-dependent and coupled to the protonation state of the Fe-bound histidines.[5] NMR investigations on a $^{15}$N-labeled Rieske protein have revealed a change of the histidines' p$K_a$ values from around 12.5 in the reduced mixed-valent cluster to around 7.4/9.1 in the oxidized diferric cluster.[6] However, mechanistic details of the hydroquinone oxidation mediated by Rieske proteins, such as the sequence or synchronism of proton and electron transfer, have remained a topic of debate.[6−9]

For many years, synthetic analogues have contributed significantly to elucidating the properties and electronic structures of biological iron−sulfur cofactors,[10] but models for the Rieske cluster have remained elusive until recently. In 2008 we reported the first (and so far only) synthetic [2Fe−2S] cluster that emulates the heteroleptic {$N_2/S_2$} ligation characteristic for the biological site, $(NEt_4)_2\mathbf{1}$ (Figure 1, left).[11] While $(NEt_4)_2\mathbf{1}$ is an excellent structural and

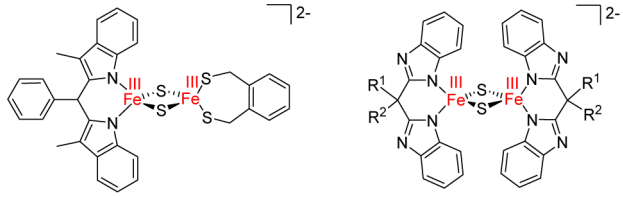


**Figure 1.** The first (and so far only) structural Rieske model **1** (left) and functional homoleptic Rieske models **2**, **3**, and **4** offering the possibility of protonation at the backside of the N-ligand (right).

**Received:** December 12, 2013
**Published:** February 7, 2014

   dx.doi.org/10.1021/ja412449v | J. Am. Chem. Soc. 2014, 136, 3946−3954

spectroscopic Rieske model in both the diferric and mixed-valent states (Mössbauer and EPR, respectively), the reduced mixed-valence species proved quite unstable and the lack of peripheral N atoms at the bis(indole) ligand in $(NEt_4)_2$**1** precluded any functional studies toward proton-coupled electron transfer (PCET).

Several robust diferric [2Fe−2S] complexes, $\mathbf{2}^{2-}$ to $\mathbf{4}^{2-}$, with homoleptic bis(benzimidazolate) ligation have been published.[12−15] In two cases these have allowed, just recently and for the first time, structural characterization of synthetic [2Fe−2S] analogues in their mixed-valent state ($\mathbf{3}^{3-}$, $\mathbf{4}^{3-}$),[13−16] and even in the super-reduced diferrous state ($\mathbf{4}^{4-}$).[16] For mixed-valent $\mathbf{2}^{3-}$ and $\mathbf{4}^{3-}$ significant valence delocalization was inferred from Mössbauer and EPR spectroscopy (about 20%, class II according to Robin and Day),[13,15] whereas the EPR spectrum of mixed-valent $\mathbf{1}^{3-}$ did not reflect delocalization to such an extent. Thus, the unique Rieske-type heteroleptic coordination of $\mathbf{1}^{3-}$ seems to promote enhanced valence localization. Homoleptic analogues $\mathbf{2}^{2-}$ to $\mathbf{4}^{2-}$ furthermore provide peripheral N atoms akin to the histidine ligands in Rieske cofactors, and their reversible protonation and their redox activity toward PCET have thus been investigated during the past two years. The twice-protonated neutral diferric cluster $\mathbf{4}H_2$ could even be isolated and structurally characterized,[15] and for both systems $\mathbf{3}^{x-}$ and $\mathbf{4}^{x-}$ thermodynamic parameters of the PCET square scheme have been elucidated.[14,15] The protonated mixed-valent species, upon reaction with TEMPO, were found to undergo concerted proton−electron transfer with rather similar rate constants on the order of $10^3$ $M^{-1}$ $s^{-1}$ under pseudo-first-order conditions at 20 °C.

An important open question now remains regarding the effect of the heteroleptic $\{N_2/S_2\}$ ligation on the PCET reaction. Here we present the first synthetic Rieske model, $\mathbf{5}^{2-}$, that comprises all beneficial features of $\mathbf{1}^{2-}$ to $\mathbf{4}^{2-}$, namely, the characteristic $\{N_2/S_2\}$ donor set that leads to enhanced valence localization in the one-electron-reduced state and a potential protonation site at the $\{N_2\}$ ligand backbone that is similar to the His-ligated subunit in the natural archetype. $\mathbf{5}^{2-}$ thus represents the highest fidelity Rieske model so far and allows for the effect of the electronic structure on the PCET reaction to be evaluated. The thermodynamic square scheme (Figure 2) is fully established, and three of the four species involved are characterized by single-crystal X-ray diffraction.

## RESULTS AND DISCUSSION

**Diferric Cluster $Fe_N^{III}Fe_S^{III}$.** Rieske model $\mathbf{5}^{2-}$ was designed with the same bis(benzimdazolate) capping ligand as was used for homoleptic cluster $\mathbf{4}^{2-}$, because this ligand proved advantageous with respect to solubility and crystallization properties. Diferric $(NEt_4)_2$**5** was synthesized via a stepwise ligand exchange reaction starting from the tetrachloro-coordinated [2Fe−2S] cluster $(NEt_4)_2[Cl_2FeS_2FeCl_2]$, in close analogy to the synthesis of the first structural Rieske model, $(NEt_4)_2$**1**.[11] To this end, phenylbis(benzimidazolyl)-methane was first deprotonated with KH and then added to a solution of $(NEt_4)_2[Cl_2FeS_2FeCl_2]$ in MeCN at −30 °C to furnish the $\{N_2\}$ cap. 1,1′-Biphenyl-2,2′-dithiolate, after deprotonation with KH, was subsequently attached as the $\{S_2\}$ capping ligand. The integrity of $\mathbf{5}^{2-}$ in solution has been supported by ESI-MS, and no ligand scrambling was observed (see the Supporting Information, Figure S1). Diffusion of diethyl ether into a solution of diferric $(NEt_4)_2$**5** in MeCN led to growth of crystals, but of rather low quality. Better quality crystals suitable for X-ray analysis could be obtained by diffusion of diethyl ether into a solution of $(CoCp^*_2)_2$**5** in MeCN at 4 °C; the molecular structure of the diferric cluster anion is shown in Figure 3.

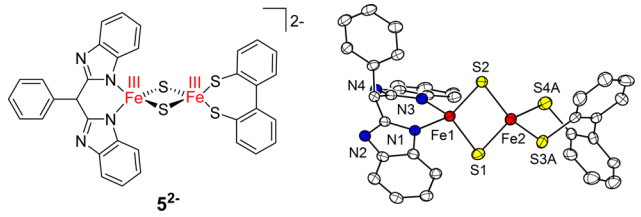


**Figure 3.** Left: schematic view of diferric cluster $\mathbf{5}^{2-}$. Right: molecular structure of the anion of $(CoCp^*_2)_2$**5** in the crystal (thermal displacement ellipsoids set at 30% probability). For clarity all hydrogen atoms have been omitted.

$(CoCp^*_2)_2$**5** crystallizes in the monoclinic space group $P2_1/c$. Selected metric parameters are listed in Table 1, together with selected data for three different biological Rieske clusters for comparison.[17−19] The Fe···Fe distance in $\mathbf{5}^{2-}$ (2.687 Å) is slightly shorter than in diferric $\mathbf{1}^{2-}$ (2.703 Å) and the biological systems (2.71−2.72 Å), but overall geometric parameters are in good agreement. Further discussion is provided below.

**Protonated Diferric Cluster H−$Fe_N^{III}Fe_S^{III}$.** To investigate the left part of the PCET square scheme (Figure 2), protonation and subsequent deprotonation experiments with diferric $(NEt_4)_2$**5** and varying acids and bases (see the Supporting Information for an overview) were followed by UV−vis spectroscopy. Addition of 1 equiv of 2,6-DMPH($BF_4$) (2,6-DMP = 2,6-dimethylpyridine) to a solution of $(NEt_4)_2$**5** in MeCN at −20 °C led to evolution of a prominent absorption band at 385 nm ($4.7 \times 10^4$ $M^{-1}$ $cm^{-1}$) (Figure 4, left), in analogy to what has been observed upon protonation of the related homoleptic [2Fe−2S] cluster $(NEt_4)_2$**4**.[15] This band has been found to indicate a tautomerism process at the particular bis(benzimidazolate) ligand, where initial protonation at one of the benzimidazolate N atoms induces migration of the bridgehead methine proton to the other peripheral benzimidazolate N atom. As a consequence, the ligand backbone becomes roughly planar and both peripheral N atoms of the benzimidazolate groups finally carry a proton (Figure 5). A similar tautomerism has previously been described for simple bis(imidazolium) compounds.[20] Furthermore, the band at 541 nm (6300 $M^{-1}$ $cm^{-1}$) for $\mathbf{5}^{2-}$ is shifted to 568 nm (6100 $M^{-1}$ $cm^{-1}$) in $\mathbf{5H}^-$, whereas the band at 450 nm (10000 $M^{-1}$ $cm^{-1}$) is shifted to lower wavelengths at 433 nm (11000 $M^{-1}$ $cm^{-1}$). Clean conversion is indicated by four isosbestic points at 556,

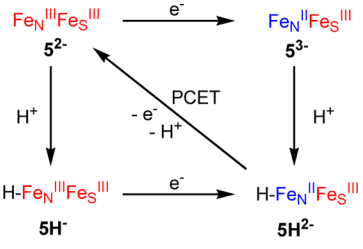


**Figure 2.** Square scheme of protonation and reduction reactions involving [2Fe−2S] Rieske model $\mathbf{5}^{x-}$. The subscripts denote the $\{N_2\}$- and $\{S_2\}$-ligated Fe sites.


dx.doi.org/10.1021/ja412449v | J. Am. Chem. Soc. 2014, 136, 3946−3954

**Table 1. Selected Bond Lengths (Å) and Angles (deg) of Diferric Clusters $(CoCp^*_2)_2$5 and $(NEt_4)_2$5H, Mixed-Valent $(NEt_4)_3$5, and Biological Rieske Clusters[17−19,a]**

| | $(CoCp^*_2)_2$5[b] | $(NEt_4)$5H | $(NEt_4)_3$5 | SOFX[17] | RIE[18] | RFS[19] |
|---|---|---|---|---|---|---|
| $d$(Fe···Fe) | 2.687(1) | 2.694(1) | 2.682(1) | 2.719 | 2.71 | 2.72 |
| $d$($Fe_N$−$\mu$-S) | 2.191(1)/2.205(1) | 2.189(1)/2.194(1) | 2.241(2)/2.248(1) | 2.258/2.259 | 2.23/2.25 | 2.28/2.31 |
| $d$($Fe_S$−$\mu$-S) | 2.200(2)/2.206(2) | 2.200(1)/2.216(1) | 2.210(2)/2.212(2) | 2.267/2.263 | 2.24/2.25 | 2.35/2.34 |
| $d$($Fe_N$−N) | 1.984(4)/1.988(4) | 1.985(2)/1.988(2) | 2.057(4)/2.074(4) | 2.100/2.083 | 2.13/2.16 | 2.19/2.23 |
| $d$($Fe_S$−S) | 2.22(2)/2.44(2), 2.37(2)/2.17(2)[b] | 2.297(1)/2.298(1) | 2.335(2)/2.345 (2) | 2.348/2.332 | 2.22/2.29 | 2.24/2.31 |
| ∠(N−$Fe_N$−N) | 91.65(16) | 92.61(10) | 86.65(17) | 92.12 | 90.78 | 90.52 |
| ∠(S−$Fe_S$−S) | 102.8(6)/106.8(5)[b] | 104.45(3) | 102.23(6) | 109.73 | 105.61 | 110.19 |
| ∠($\mu$S−$Fe_N$−$\mu$-S) | 104.88(6) | 104.90(3) | 104.68(6) | 106.24 | 105.62 | 109.14 |
| ∠($\mu$S−$Fe_S$−$\mu$-S) | 104.57(6) | 103.80(3) | 106.95(6) | 105.81 | 105.64 | 105.70 |

[a]SOFX = Rieske protein II from *Sulfolobus acidocaldarius*, RIE = soluble domain of Rieske protein from bovine mitochondrial $bc_1$ complex, and RFS = soluble domain of Rieske protein from spinach chloroplast $b_6f$ complex. [b]Disordered {$S_2$} ligand (see the Supporting Information for details); the true $Fe_S$−S bond length likely is an average value, 2.30 Å.

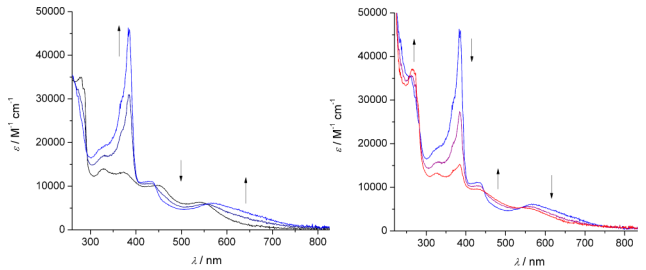


**Figure 4.** Left: addition of 0.5 (dark blue) and 1.0 (blue) equiv of 2,6-DMPH($BF_4$) to $5^{2-}$ (black) in MeCN at −20 °C, generating $5H^-$. Right: further addition of 0.5 (purple) and 1.0 (red) equiv of 2,6-DMPH($BF_4$) to $5H^-$ (blue), generating $5H_2$.

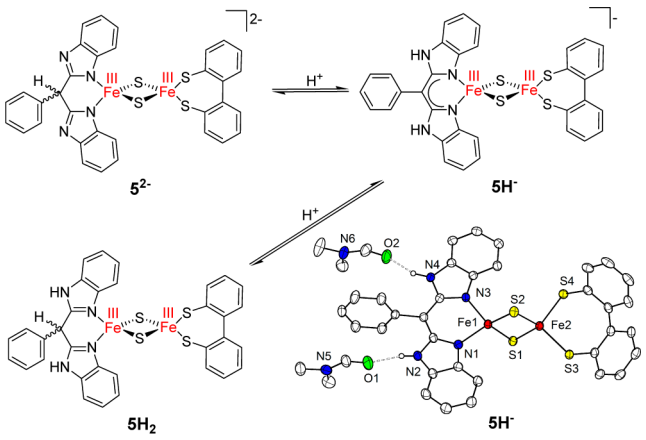


**Figure 5.** Protonation of diferric $5^{2-}$ leading to the reversible formation of $5H^-$ and $5H_2$. Lower right: molecular structure of the anion of $(NEt_4)$5H·2DMF·$Et_2O$ in the crystal (thermal displacement ellipsoids set at 30% probability). For clarity all hydrogen atoms except the N−H atoms, which are hydrogen bonded to the two DMF molecules, have been omitted.

442, 293, and 265 nm. Protonation to give $5H^-$ proved to be reversible, since the original spectrum of $5^{2-}$ was restored upon addition of base (either diazabicycloundecane (DBU) or phosphazene base 1-*tert*-butyl-2,2,4,4,4-pentakis-(dimethylamino)-2$\lambda^5$,4$\lambda^5$-catenadiphosphazene (*t*-BuP2); see the Supporting Information for formulas and abbreviations and Figure S5 in the Supporting Information for the back-titration).

In contrast to 2,6-DMPH($BF_4$), addition of 1 equiv of 2,2,6,6-TMPH($BF_4$) (2,2,6,6-TMP = 2,2,6,6-tetramethylpiperidine) to a solution of $(NEt_4)_2$5 in DMF did not lead to full conversion to $5H^-$, but 4 equiv is needed. We conclude that the p$K_a$ of 2,2,6,6-TMPH($BF_4$) in DMF (≥19) is in the same range as the p$K_a$ of $5H^-$ and thus is too low to achieve full protonation. Interestingly, $\lambda_{max}$ of the absorption characteristic for the tautomerized ligand is shifted by about 5 nm if the reaction is carried out in DMF instead of MeCN, suggesting the involvement of solvent molecules in H-bonding. This, as well as the tautomerism discussed above, has been confirmed by the X-ray diffraction analysis of singly protonated diferric cluster $(NEt_4)$5H, which could be crystallized via DMF/$Et_2O$ diffusion at 4 °C. The solid-state structure clearly shows hydrogen bonds between the protonated benzimidazolate N and DMF solvent molecules included in the crystal lattice (Figure 5, bottom right). After crystallographic characterization of twice-protonated $4H_2$,[16] this represents the second synthetic [2Fe−2S] cluster that could be isolated in protonated form and the first that also emulates the protonated Rieske cluster with its heteroleptic ligation. Geometric parameters of the cluster core remain almost unchanged upon protonation (see Table 1), which will be discussed below.

Addition of a second equivalent of 2,6-DMPH($BF_4$) (Figure 4, right) led to disappearance of the band at 385 nm characteristic for $5H^-$ that had emerged during the first protonation event. This observation led us to conclude that binding of a second proton to give $5H_2$ is possible and restores the original situation at the C atom bridging the two benzimidazolate moieties, disrupting conjugation within the {$N_2$} capping ligand just as in $5^{2-}$ (Figure 5). Clean conversion is indicated by four isosbestic points at 537, 447, 283, and 258 nm. Shifts of the other absorptions are relatively minor. However, the product $5H_2$ seemed to be unstable in MeCN at −20 °C, and upon addition of DBU minor decomposition was detected by the appearance of a new band at 424 nm concomitant with broadening of all bands, especially in the region at about 540 nm (see Figure S6 in the Supporting Information).

Following the protonation events by $^1$H NMR in MeCN-$d_3$ at room temperature showed the formation of a new signal at about 14 ppm which has been attributed to the formation of an NH group. Furthermore, the double set of signals for the {$N_2$} capping ligand turned into a single set, clearly revealing the flattening of the bis(benzimidazolate) scaffold with resulting 2-fold symmetry in $5H^-$ (see Figures S3 and S4 in the Supporting Information for NMR spectra). The process is almost reversible upon addition of *t*-BuP2, though formation of minor amounts


dx.doi.org/10.1021/ja412449v | J. Am. Chem. Soc. 2014, 136, 3946−3954

of free ligand and an unknown paramagnetic species evidence the limited stability of $5H^-$ in solution at room temperature. Addition of a second equivalent of 4-DMAPH(OTf) (4-DMAP = 4-(dimethylamino)pyridine) did not lead to spectral changes at −30 °C, suggesting that 4-DMAPH$^+$ ($pK_a$ = 17.95)[21] is a weaker acid than $5H_2$, in contrast to 2,6-DMPH$^+$ ($pK_a$ = 14.13).[21]

The $pK_a$ value of diferric $5H^-$, relevant for establishing the square scheme in Figure 2, has been determined by protonation of $5^{2-}$ with 1 equiv of 2,6-DMPH($BF_4$) and back-titration with DBU ($pK_a$ = 24.34)[21] in MeCN followed by UV−vis spectroscopy under inert conditions at room temperature. According to mass balance, a $pK_a$ of 23.6 ± 0.3 was thus derived (see the Supporting Information for details).

**Mixed-Valent Cluster $Fe_N^{II}Fe_S^{III}$.** Electrochemical properties of $5^{2-}$ were studied by cyclic voltammetry in MeCN/0.1 M $NBu_4PF_6$ at various scan rates and at room temperature (Figure 6, left). The cluster undergoes two cathodic redox processes:

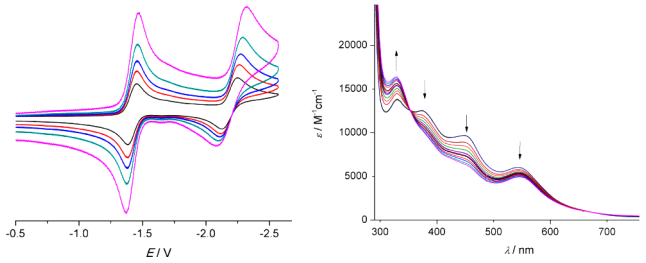


**Figure 6.** Left: cyclic voltammogram of $5^{2-}$ ($c$ = 1.0 mM) in MeCN/0.1 M $Bu_4NPF_6$ at rt vs Fc/Fc$^+$. $E_1$ = −1.43 V and $E_2$ = −2.19 V at various scan rates ($v$ = 100, 200, 300, 500, and 1000 mV s$^{-1}$). Right: electrochemical reduction of $5^{2-}$ in MeCN/0.1 M $Bu_4NPF_6$ at rt at a potential of −1.6 V. The course of reduction was followed by UV−vis spectroscopy.

the first chemically reversible reduction occurs at $E_{1/2}{}^1$ = −1.43 V and the second quasi reversible reduction at $E_{1/2}{}^2$ = −2.19 V (vs Fc/Fc$^+$). From the separation of the two redox waves a conproportionation constant $K_c$ = 7.1 × 10$^{12}$ can be derived. While $K_c$ is 4 orders of magnitude smaller than the value calculated for $4^{3-}$,[13] the stability of mixed-valent $5^{3-}$ against disproportion is still relatively high.

Mixed-valent $5^{3-}$ was thus generated by bulk electrolysis starting from diferric $5^{2-}$ in MeCN/0.1 M $Bu_4NPF_6$ at room temperature at an applied potential of −1.6 V. The course of reduction was followed by UV−vis spectroscopy (Figure 6, right), and clean conversion is reflected by an isosbestic point at 353 nm. Reduction led to an overall decrease of intensity in the visible region of the spectrum, the band at 543 nm dropping to 4900 M$^{-1}$ cm$^{-1}$. Only a band at 330 nm assigned to a ligand to metal charge transfer (LMCT) deriving from the {$S_2$} ligand increased in intensity (16300 M$^{-1}$ cm$^{-1}$). Both bands at 374 and 447 nm, assigned to CT transitions from the {$N_2$} ligand by comparison with homoleptic $5^{2-}$,[13,15] almost vanished, suggesting that the reduction is localized at the {$N_2$}-ligated iron atom.

In another experiment after 50% of the reduction was completed (to ensure that side products had not been formed yet), a sample was taken and investigated by EPR spectroscopy (Figure 7). The total spin of the mixed-valent species $S_T$ = 1/2 caused by antiferromagnetic coupling of $Fe^{III}$ and $Fe^{II}$ gives rise to a characteristic rhombic EPR spectrum. Simulation of the

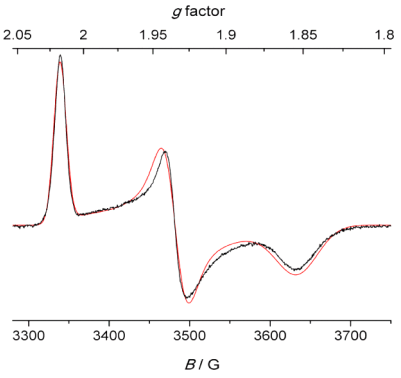


**Figure 7.** EPR spectrum of $5^{3-}$ in MeCN/0.1 M $Bu_4NPF_6$ measured as frozen glass at 20 K. The red line is a powder simulation with $g$ = 2.017, 1.934, and 1.854 and Gaussian line widths Γ = 8.5, 14, and 26 G.

spectrum gave $g$ values of 2.017, 1.934, and 1.854, with an *average* value $g_{av}$ = 1.935.

In accordance with the UV−vis results, the wide $g$ anisotropy of the EPR spectrum indicates that the unpaired electron in $5^{3-}$ is largely localized at the {$N_2$}-coordinated iron atom,[22] in analogy to what has been observed for reduced Rieske cofactors. Table 2 compares $g$ values for a series of natural

**Table 2. EPR Data of Model Complexes $5^{3-}$, $1^{3-}$, and $4^{3-}$ and Selected Rieske Proteins[25−27,a]**

| | $5^{3-}$ | $1^{3-}$ | $4^{3-}$ | *Tt*[25] | ISP $bc_1$[26] | Cyt $b_6f$[27] |
|---|---|---|---|---|---|---|
| $g_1$ | 2.017 | 2.015 | 2.015 | 2.02 | 2.024 | 2.03 |
| $g_2$ | 1.934 | 1.936 | 1.937 | 1.90 | 1.89 | 1.90 |
| $g_3$ | 1.854 | 1.803 | 1.900 | 1.80 | 1.79 | 1.76 |
| $g_{av}$ | 1.935 | 1.918 | 1.951 | 1.91 | 1.90 | 1.90 |

[a] *Tt* = Rieske protein of *Thermus thermophilus*, ISP $bc_1$ = bovine mitochondrial Cyt $bc_1$, and Cyt $b_6f$ = cytochrome $b_6f$ complex from spinach.

and synthetic [2Fe−2S] clusters. Biological Rieske clusters usually show an average value $g_{av}$ of 1.90−1.91,[23] whereas higher values are observed for common all-cysteinato-ligated [2Fe−2S] ferredoxins ($g_{av}$ = 1.945−1.975).[23] As Mouesca has pointed out, electronic delocalization in [2Fe−2S] clusters tends to increase the average $g$ value, $g_{av} = {}^1/_3\sum g_i$, toward the free electron value ($g$ = 2.0023).[24] Therefore, the value $g_{av}$ = 1.935 reflects increased valence localization in $5^{3-}$ compared to the synthetic homoleptic {$N_2/N_2$} analogues $2^{3-}$ ($g_{av}$ = 1.940 in DMF/0.25 M *n*-$BuNClO_4$, 77 K)[12] and $4^{3-}$ ($g_{av}$ = 1.951 in DMF, 6 K),[13] but electron localization is less pronounced than in $1^{3-}$ ($g_{av}$ = 1.918).[11]

Increased valence localization in the new Rieske model $5^{3-}$, if compared to previous homoleptic Rieske models $2^{3-}$ and $4^{3-}$ with two bis(benzimidazolate) capping ligands in their mixed-valent states, reflects the reduced symmetry of the complex and the heteroleptic {$S_2/N_2$} ligation, which leads to site preference of the unpaired electron. Furthermore, the negatively charged thiolate ligand is a $\sigma$- and $\pi$-donor, which stabilizes the higher oxidation state ($Fe^{III}$). Hence, the new model $5^{3-}$ more closely emulates the electronic situation of the biological antetype than previous models $2^{3-}$ and $4^{3-}$.

The mixed-valent cluster was generated chemically by reduction of $(NEt_4)_2$**5** with $CoCp^*_2$ in DMF at −20 °C, giving microcrystalline $(CoCp^*_2)(NEt_4)_2$**5**. Crystalline material


dx.doi.org/10.1021/ja412449v | J. Am. Chem. Soc. 2014, 136, 3946−3954

of mixed-valent $(NEt_4)_3$**5** could be obtained from DMF after addition of 1 equiv of $NEt_4Br$ and subsequent slow diffusion of $Et_2O$ at 4 °C into the solution. $(NEt_4)_3$**5** crystallizes in the monoclinic space group $P2_1/n$ and represents the first exact Rieske model with heteroleptic $\{N_2/S_2\}$ ligation that has been characterized by X-ray diffraction in the reduced state. This now allows a unique comparison of the molecular structures of a high-fidelity synthetic analogue for the Rieske cluster in three relevant forms, namely, in the diferric $\mathbf{5}^{2-}$, the diferric protonated $\mathbf{5H}^{-}$, and the mixed-valent $\mathbf{5}^{3-}$ states. Inspection of the central [2Fe−2S] core shows that only minor changes occur upon reduction or protonation (Figure 8), with the Fe···

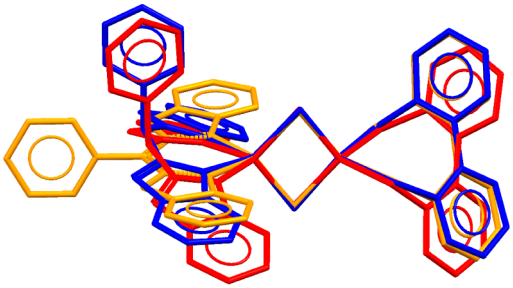

**Figure 8.** Overlay of the molecular structures of diferric $\mathbf{5}^{2-}$ (red), mixed-valent $\mathbf{5}^{3-}$ (blue), and protonated diferric $\mathbf{5H}^{-}$ (yellow).

Fe distance showing negligible variations (<0.02 Å). This reflects the low reorganization energies of [2Fe−2S] clusters that make them favorable electron transfer cofactors in biology. Close comparison of the subtle structural changes upon reduction ($\mathbf{5}^{2-}$ versus $\mathbf{5}^{3-}$) is interesting, however, because it reveals that changes mainly occur around the $\{N_2\}$-coordinated iron atom: bonds between $Fe_N$ and the $\mu$-S elongate by ∼0.05 Å upon reduction, while bonds between $Fe_S$ and the $\mu$-S remain essentially unchanged (<0.01 Å). Interestingly, in the case of homoleptic $\{N_2\}$-capped $\mathbf{3}^{2-}/\mathbf{3}^{3-}$ and $\mathbf{4}^{2-}/\mathbf{4}^{3-}$, the bonds between both Fe atoms and the $\mu$-S lengthen by ∼0.03 Å upon reduction, showing that the unpaired electron is delocalized in $\mathbf{4}^{3-}$ (on the crystallographic time scale), but is largely localized at the single $\{N_2\}$-coordinated iron site in $\mathbf{5}^{3-}$. In line with these considerations reduction of $\mathbf{5}^{2-}$ leads to a more pronounced lengthening of the bonds between $Fe_N$ and the $\{N_2\}$ capping ligand (0.08 Å) than for the bonds between $Fe_S$ and the $\{S_2\}$ capping ligand (0.04 Å). Fe−N bonds in the homoleptic $\{N_2\}$-capped clusters show averaged elongations of 0.07 Å ($\mathbf{3}^{2-}/\mathbf{3}^{3-}$) or 0.05 Å ($\mathbf{4}^{2-}/\mathbf{4}^{3-}$). The most prominent structural difference was found for the N−$Fe_N$−N angle, which shrinks by around 5° in mixed-valent $\mathbf{5}^{3-}$ compared to diferric $\mathbf{5}^{2-}$ and $\mathbf{5H}^{-}$. All these crystallographic findings, though subtle, corroborate that reduction of the Rieske model occurs at the $Fe_N$ site in accordance with EPR and Mössbauer spectroscopy (see below). Selected geometric parameters are compiled in Table 1.

The zero-field Mössbauer spectrum of diferric $(NEt_4)_2$**5** shows two quadrupole doublets at a ratio of 1:1 with isomeric shifts $\delta_1$ = 0.26 mm $s^{-1}$ and $\delta_2$ = 0.28 mm $s^{-1}$, as expected for two distinct ferric sites (Figure 9, left). Differences in quadrupole splitting allow an assignment to the all-sulfur-coordinated $Fe_S$ ($\Delta E_{Q1}$ = 0.52 mm $s^{-1}$) and the $\{N_2\}$-capped $Fe_N$ ($\Delta E_{Q2}$ = 1.16 mm $s^{-1}$); the larger quadrupole splitting in the case of $Fe_N$ reflects the increased electric field gradient resulting from the higher asymmetry of electronic charge

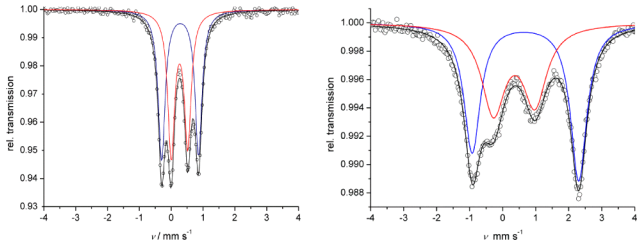


**Figure 9.** Zero-field Mössbauer spectra of solid $(NEt_4)_2$**5** (left) and $(CoCp^*)(NEt_4)_2$**5** (right) at 80 K. Simulation of the data gave the following parameters: (left) $\delta_1$ = 0.26 mm $s^{-1}$ and $\Delta E_{Q1}$ = 0.52 mm $s^{-1}$ (red), $\delta_2$ = 0.28 mm $s^{-1}$ and $\Delta E_{Q2}$ = 1.16 mm $s^{-1}$ (blue); (right) $\delta_1$ = 0.35 mm $s^{-1}$ and $\Delta E_{Q1}$ = 1.26 mm $s^{-1}$ (red), $\delta_2$ = 0.69 mm $s^{-1}$ and $\Delta E_{Q2}$ = 3.23 mm $s^{-1}$ (blue).

distribution. Overall the Mössbauer data show good agreement with parameters found for $(NEt_4)_2$**1** and biological Rieske clusters (see Table S2 in the Supporting Information).

Variable-temperature zero-field Mössbauer spectra of mixed-valent $(CoCp^*_2)(NEt_4)_2$**5** show two doublets at a ratio of about 1:1 in the range from 6 to 200 K, as expected for a mixed-valent [2Fe−2S] cluster with heteroleptic terminal coordination (spectrum at 80 K shown in Figure 9 (right), spectra at 6 and 200 K shown in the Supporting Information; see also Table S3 in the Supporting Information). The doublets can be assigned to the $\{N_2\}$-coordinated $Fe_N$ atom with an isomeric shift typical for $Fe^{II}$ and a large quadrupole splitting ($\delta_2$ = 0.69 mm $s^{-1}$, $\Delta E_{Q2}$ = 3.23 mm $s^{-1}$, 80 K) and to the $\{S_2\}$-coordinated $Fe^{III}$ atom featuring a smaller isomeric shift and smaller splitting ($\delta_1$ = 0.35 mm $s^{-1}$, $\Delta E_{Q1}$ = 1.26 mm $s^{-1}$, 80 K). These values are in good agreement with data for biological Rieske cofactors, though quadrupole splittings $\Delta E_Q$ are somewhat smaller for the latter (Table 3). In contrast to

**Table 3. Mössbauer Parameters (mm $s^{-1}$) of $(CoCp^*_2)(NEt_4)_2$5 and Biological Rieske Clusters in the Reduced State[a]**

| | $(CoCp^*_2)(NEt_4)_2$**5**, 6 K | *Tt*,[25] 4.2 K | ISP,[29] 4.2 K | T4MOC,[30] 4.2 K |
|---|---|---|---|---|
| $\delta_1$ | 0.34 | 0.31 | 0.25 | 0.30 |
| $\delta_2$ | 0.70 | 0.74 | 0.73 | 0.72 |
| $\Delta E_{Q1}$ | 1.29 | 0.63 | 0.70 | 0.71 |
| $\Delta E_{Q2}$ | 3.24 | 3.05 | 2.95 | 3.07 |
| $\Delta\delta$ | 0.36 | 0.43 | 0.48 | 0.42 |

[a] *Tt* = Rieske protein of *Thermus thermophilus*, ISP = Rieske protein of Cyt *bf* complex from spinach, and T4MOC = Rieske protein from *Pseudomonas mendocina* in *Escherichia coli*.

mixed-valent $(NEt_4)_3$**2** and $(NEt_4)_3$**4**, in which cases the two quadrupole doublets collapsed to a single quadrupole doublet at 200 K, electron hopping on the Mössbauer time scale cannot be observed for $(CoCp^*_2)(NEt_4)_2$**5**.

An empirical correlation for $\delta$ and the oxidation number ($x$) of $FeS_4$ units $\delta(x)$ = (1.43 − 0.40$x$) mm $s^{-1}$ has been reported.[28] This would predict values of $\delta$(III) = 0.23 mm $s^{-1}$ and $\delta$(II) = 0.63 mm $s^{-1}$ and hence a difference of 0.4 mm $s^{-1}$ for fully localized ferric and ferrous sites a and b. While for homoleptic mixed-valent $\mathbf{4}^{3-}$ only half as much ($\Delta\delta$ = 0.22 mm $s^{-1}$ at 4 K)[13,15] was observed, the present heteroleptic Rieske model $\mathbf{5}^{3-}$ gives $\Delta\delta$ = 0.36 mm $s^{-1}$ at 6 K (0.34 mm $s^{-1}$ at 80 K), close to the expected value. Though this is still less than $\Delta\delta$ in the range 0.42−0.48 mm $s^{-1}$ observed for biological Rieske


dx.doi.org/10.1021/ja412449v | J. Am. Chem. Soc. 2014, 136, 3946−3954

sites featuring full valence localization (Table 3), it reflects the increased valence localization in $5^{3-}$ compared to previous homoleptic models, in accordance with EPR data.

**Protonation of Mixed-Valent Cluster $Fe_N^{II}Fe_S^{III}$.** Protonation of the mixed-valent cluster proved to be challenging because of low stability of the resulting species. Instantaneous degradation could be observed upon protonation at room temperature. At −30 °C in MeCN the addition of 1 equiv of 2,6-DMPH($BF_4$) could be followed by UV−vis spectroscopy (see Figure S7 in the Supporting Information), and only minor absorption changes were detected: The band at 328 nm ($2.4 \times 10^4$ $M^{-1}$ $cm^{-1}$) drops by about 3000 $M^{-1}$ $cm^{-1}$, whereas absorption in the region between 350 and 650 nm rises by about 2000 $M^{-1}$ $cm^{-1}$. The maximum at 550 nm (4800 $M^{-1}$ $cm^{-1}$) broadens and experiences a slight red shift (5500 $M^{-1}$ $cm^{-1}$). If handled at −30 °C throughout, addition of *t*-BuP2 did lead to nearly full conversion back to the original spectrum of $5^{3-}$. Since no intense band around 385 nm evolved upon protonation of $5^{3-}$, it can be assumed that mixed-valent $5H^{2-}$ does not undergo any tautomerism that was observed for diferric $5H^-$ .

EPR spectra of the singly protonated species $5H^{2-}$ showed a rhombic spectrum with *g* values of 1.994, 1.938, and 1.875 ($g_{av}$ = 1.937), but with rather large line widths (60, 33, and 55 G) even when spectra were recorded at low temperatures (10 K; see the Supporting Information). The reasons for this are unclear; a more detailed investigation and comparative analysis of the EPR spectra of $4^{3-}$ and $5^{3-}$ and their protonated forms is currently in progress.

The effect of protonation on the redox potentials was investigated by cyclic voltammetry, focusing on the first reduction wave that appears at $E_{1/2}$ = −1.43 V vs $Fc/Fc^+$ for $5^{2-}$ (Figure 10). Addition of 1 equiv of 4-DMAPH(OTf) led to the emergence of a new cathodic peak at $E_p^c$ = −1.27 V, which is anodically shifted by +230 mV compared to the cathodic peak potential of the reversible couple for $5^{2-}$ ($E_p^c$ = −1.50 V). This leads to an estimated redox potential of −1.20 V for protonated $5H^-$ (assuming a similar shift $E_p^c - E_{1/2}$ for $5^{2-}$ and $5H^-$). However, protonation obviously is not complete upon addition of 1 equiv of 4-DMAPH(OTf), since the original peak at $E_p^c$ = −1.50 V is still discernible. Addition of a second equivalent of 4-DMAPH(OTf) caused the peak at $E_p^c$ = −1.50 V to disappear, concomitant with a broadening of the peak at $E_p^c$ = −1.27 V assigned to $5H^-$ and emergence of a third redox event characterized by a peak at $E_p^c$ = −1.02 V, shifted anodically by +480 mV compared to $5^{2-}$ ($E_p^c$ = −1.50 V). The additional peak presumably reflects the presence of some twice-protonated species $5H_2$. When base was then added, the original redox wave characteristic of $5^{2-}$ ($E_p^c$ = −1.50 V, $E_{1/2}$ = −1.43 V) reappeared, confirming chemical reversibility of the protonation events (Figure 10).

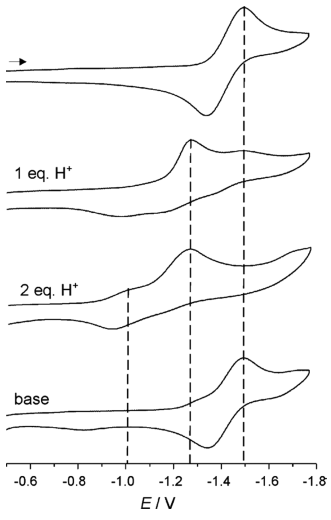


**Figure 10.** Cyclic voltammogram of $(NEt_4)_2$**5** (*c* = 1.0 mM) in MeCN/0.1 M $Bu_4NPF_6$ at rt vs $Fc/Fc^+$ at a scan rate of 500 mV/s (top). The redox potential is shifted upon addition of acid (second and third pictures from top). Subsequent addition of *t*-BuP2 proves the reversibility of the process (bottom).

The anodic shift of about +480 mV upon 2-fold protonation of $5^{2-}$ is more than twice as large as the shift observed for homoleptic clusters $3^{2-}$ and $4^{2-}$ after binding of two protons (+240 and +200 mV, respectively).[14,15] The difference reflects that the two protons are bound to the same bis(benzimidazole) ligand at the unique $Fe_N$ site in $5H_2$, in close analogy to the situation in Rieske proteins, while the two protons are bound to two bis(benzimidazole) ligands at different Fe sites in homoleptic $3H_2$ and $4H_2$. Indeed, a shift of +300 to +440 mV upon going from very low to very high pH (hence going from the twice-protonated to the fully deprotonated form) has been reported for biological Rieske clusters depending on the type of protein;[31] redox potentials for the intermediate singly protonated forms have not yet been reported. Hence, the electrochemical response to protonation for the synthetic analogue $5^{2-}$ nicely emulates the properties of the biological antetype.

To establish a thermodynamic square scheme for the new Rieske model, not only redox potentials but also the p$K_a$ value of mixed-valent $5H^{2-}$ was determined (Figure 11). To this end

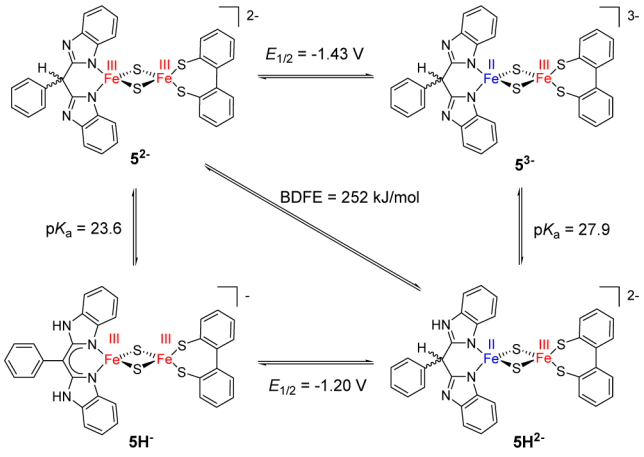


**Figure 11.** Square scheme summarizing thermodynamic parameters for the second-generation Rieske model cluster in MeCN with potentials referenced against $Fc/Fc^+$.

$5^{3-}$ was protonated with 1 equiv of 4-DMAPH($BF_4$) in MeCN-$d_3$ at low temperatures, and back-titration with phosphazene base (*tert*-butylimino)tris(1-pyrrolidinyl)phosphorane (*t*-BuP1-(pyrr)) (p$K_a$ = 28.42) was followed by $^1$H NMR at room temperature (see the Supporting Information for details, Figures S11 and S12). A p$K_a$ of 27.9 ± 0.2 was thus determined for $5H^{2-}$ in MeCN. In comparison to the homoleptic model complex $3^{3-}$ (p$K_a$ = 24.7 ± 0.4), the present heteroleptic Rieske-type cluster $5^{3-}$ is more basic, probably due to the


dx.doi.org/10.1021/ja412449v | J. Am. Chem. Soc. 2014, 136, 3946−3954

increased valence localization and the more pronounced ferrous character at the protonation site. p$K_a$ values of reduced Rieske proteins (12.3−13.3; see above) are much lower than those of $\mathbf{5}^{3-}$ and $\mathbf{3}^{3-}$. The comparability is limited, however, since those values for Rieske proteins have been determined in aqueous solution, and they are tuned by interactions with the surrounding protein environment comprising, for instance, several hydrogen bonds.[32]

The bond dissociation free energy (BDFE) of the N−H bond of the protonated cluster $\mathbf{5H}^{2-}$ can be calculated from the available p$K_a$ and $E_{1/2}$ data (see the Supporting Information),[33] giving BDFE = 60.2 ± 0.5 kcal mol$^{-1}$ (252 ± 2 kJ mol$^{-1}$). This BDFE for the NH bond is close to the value found for the related homoleptic model complex $\mathbf{3H}^{2-}$ (60.5 kcal mol$^{-1}$),[14] but about 10 kcal mol$^{-1}$ less than that of Rieske protein *Rs*Rp under basic conditions (71.5 kcal mol$^{-1}$) and even 15 kcal mol$^{-1}$ less than the value obtained for the protonated form of *Rs*Rp under acidic conditions (75.1 kcal mol$^{-1}$).[5e,33] The lower BDFE, hence the weaker N−H bond in the model complexes, is likely related to the differently charged ligands in the mixed-valent state, namely, neutral histidines versus monoanionic bis(benzimidazolate). The very similar BDFE values for $\mathbf{3H}^{2-}$ and $\mathbf{5H}^{2-}$ evidence that heteroleptic ligation of the [2Fe−2S] core does not play any role in this respect.

With those values at hand, a p$K_a$ of about 23.8−24.2 could be calculated for diferric $\mathbf{5H}^{-}$ according to Hess's law (see the Supporting Information). This is in good agreement with the value determined experimentally by UV−vis titration of $\mathbf{5H}^{-}$ with DBU, 23.6 ± 0.3 as described above. The difference in p$K_a$ for mixed-valent $\mathbf{5H}^{2-}$ and diferric $\mathbf{5H}^{-}$ of about 4 units is in accord with the change of the histidines' p$K_a$ values from around 12.5 in the reduced mixed-valence forms to around 7.4/9.1 in the oxidized diferric forms of Rieske proteins.[5]

To examine its PCET reactivity, mixed-valent $\mathbf{5H}^{2-}$ (generated in situ by addition of 1 equiv of 4-DMAPH($BF_4$) to $\mathbf{5}^{3-}$) was treated with the nitroxyl radical TEMPO. Full conversion to deprotonated diferric $\mathbf{5}^{2-}$ and 1 equiv of TEMPO-H was ascertained by $^1$H NMR spectroscopy. Because of the moderate N−H BDFE of $\mathbf{5H}^{2-}$, calculation of the free energy of the reaction, $\Delta G^\circ_{CPET}$ (CPET = concerted proton and electron transfer), gives a sizable value, −26.4 kJ mol$^{-1}$ (see the Supporting Information). To obtain mechanistic insight, double-mixing stopped-flow measurements were undertaken at varying temperatures under pseudo-first-order conditions using an excess of TEMPO, yielding kinetic parameters of the reaction (see the Supporting Information). At 20 °C, a second-order rate constant $k$ = (9.5 ± 1.2) × 10$^4$ M$^{-1}$ s$^{-1}$ was determined, and the transition-state parameters $\Delta H^\ddagger$ = 8.7 ± 1.0 kJ mol$^{-1}$ and $\Delta S^\ddagger$ = −120 ± 40 J mol$^{-1}$ K$^{-1}$ were derived from an Eyring plot (Figure S15, Supporting Information). For the free energy of the transition state, $\Delta G^\ddagger$, at 293 K a value of 43.8 ± 0.3 kJ mol$^{-1}$ was thus calculated (see the Supporting Information).

To verify that the reaction follows a concerted and not a stepwise pathway, the initial steps of the alternative pathways were examined. These are, starting from $\mathbf{5H}^{2-}$ and TEMPO, either proton transfer or electron transfer, leading to $\mathbf{5}^{3-}$ (and TEMPO-H$^{\bullet+}$) or $\mathbf{5H}^{-}$ (and TEMPO$^-$), respectively. To ascertain the favored pathway, the respective activation energies have been compared. Since the activation energies $\Delta G^\ddagger$ must be at least as high as the free energies $\Delta G^\circ_{CPET}$, these values are a conservative lower limit to $\Delta G^\ddagger$ (for calculation of the free energies $\Delta G^\circ_{PT}$ and $\Delta G^\circ_{ET}$, see the Supporting Information). Since $\Delta G^\circ_{PT}$ = 184 kJ mol$^{-1}$ and $\Delta G^\circ_{ET}$ = 72.4 kJ mol$^{-1}$ are larger than the activation energy for the concerted pathway ($\Delta G^\ddagger$ = 43.8 kJ mol$^{-1}$), the stepwise pathways can be excluded.

$\Delta G^\ddagger$ for $\mathbf{5H}^{2-}$is about 10 kJ mol$^{-1}$ smaller compared to the value for cluster $\mathbf{3H}^{2-}$;[14] therefore, the rate constant at room temperature is more than 1 order of magnitude higher for heteroleptic $\mathbf{5H}^{2-}$ than for homoleptic $\mathbf{3H}^{2-}$. $\Delta H^\ddagger$ is of the same order of magnitude (about 2 kJ mol$^{-1}$ larger), while $\Delta S^\ddagger$ for $\mathbf{5H}^{2-}$ is less negative than for $\mathbf{3H}^{2-}$.[14] The transition-state parameter $\Delta H^\ddagger$ obtained for homoleptic $\mathbf{4H}^{2-}$ is at least twice as large as the value found for $\mathbf{5H}^{2-}$ (Table 4),[15] because the second-order rate constant is about 2 orders of magnitude lower than the one derived for $\mathbf{5H}^{2-}$.

**Table 4. Thermodynamic and Kinetic Parameters for the Reactions of TEMPO with $\mathbf{3H}^{2-}$, $\mathbf{4H}^{2-}$, and $\mathbf{5H}^{2-}$**

| | $\mathbf{4H}^{2-}$[15] (in DMF) | $\mathbf{3H}^{2-}$[14] (in MeCN) | $\mathbf{5H}^{2-}$ (in MeCN) |
|---|---|---|---|
| $\Delta H^\ddagger$ (kJ mol$^{-1}$) | 17.6 ± 0.6 | 6.7 ± 1.3 | 8.7 ± 1.0 |
| $\Delta S^\ddagger$ (J mol$^{-1}$ K$^{-1}$) | −130 ± 2 | −159 ± 10 | −120 ± 5 |
| $k$ at 20 °C (M$^{-1}$ s$^{-1}$) | 722 ± 14 | 2200 ± 350[a] | 95000 ± 12000 |
| $\Delta G^\ddagger$ at 20 °C (kJ mol$^{-1}$) | 55.7 ± 1.1 | 54.0 ± 1.2 | 43.8 ± 0.3 |
| BDFE(Fe−H) (kJ mol$^{-1}$) | | 253 ± 4 | 252 ± 2 |
| $\Delta G^\circ_{CPET}$ (kJ mol$^{-1}$) | | −25.1 | −26.4 |

[a]At 25 °C.

The differences in activation parameters and in rate constant $k$ for the closely related complexes $\mathbf{3H}^{2-}$ and $\mathbf{4H}^{2-}$, both with homoleptic bis(benzimidazolate) ligation, can likely be attributed to the different solvents used in those studies.[14,15] Polar solvents such as DMF can interact with both reaction partners, presumably decelerating the reaction; H-bonding interaction between DMF and the N−H units of $\mathbf{4H}_2$ had indeed been detected by X-ray crystallography and by IR spectroscopy,[15] similar to what is seen here for the structure of $\mathbf{5H}^{-}$ in the solid state (vide supra). The significantly different rate constants $k$ for $\mathbf{3H}^{2-}$ and $\mathbf{5H}^{2-}$, both measured in MeCN solution, may appear counterintuitive at first sight, since $\Delta G^\circ_{CPET}$ = −6.0 kcal mol$^{-1}$ (−25.1 kJ mol$^{-1}$) found for $\mathbf{3H}^{2-}$ is quite similar to the value determined for $\mathbf{5H}^{2-}$. The much lower activation energy $\Delta G^\ddagger$ that leads to accelerated PCET in the case of $\mathbf{5H}^{2-}$, however, might be an effect of increased localization of electron density in the Rieske-type [2Fe−2S] core with its heteroleptic {$N_2$/$S_2$} ligation. It should be noted that Fe−N bonds, upon reduction, elongate almost equally in $\mathbf{5}^{2-}$ and in homoleptic $\mathbf{3}^{2-}$, while the $Fe_S$−S bonds in $\mathbf{5}^{2-}$ change much less. This might give rise to a smaller reorganization energy, $\lambda$, during PCET, which in turn leads to faster PCET between the cluster and TEMPO. It has been shown before that Marcus's theory, which had initially been established for ET reactions, can also be applied to PCET reactions.[34,35] Thus, a small reorganization energy $\lambda$ should be advantageous not only for fast electron transfer, but for fast PCET as well. However, at present it cannot be excluded that steric effects, viz., a different TEMPO accessibility of the backbone N−H groups caused by different substituents at the nearby bridging C atom (Ph/H in $\mathbf{5H}^{2-}$ versus *n*-Pr/*n*-Pr in $\mathbf{3H}^{2-}$), may also play a role; see Figure S19 in the Supporting Information for illustrative space-filling models generated from the crystal structures of mixed-valent $\mathbf{3}^{3-}$ and $\mathbf{5}^{3-}$.


dx.doi.org/10.1021/ja412449v | *J. Am. Chem. Soc.* 2014, 136, 3946−3954

## CONCLUSIONS

In summary, we report a synthetic analogue for the Rieske cofactor that not only emulates the heteroleptic $\{His_2Cys_2\}$ ligation of the biological antetype, but also represents a functional model undergoing fast concerted electron and proton transfer. All four species in the PCET square scheme have been thoroughly characterized, and three of them, namely, diferric $\mathbf{5}^{2-}$, protonated diferric $\mathbf{5H}^{2-}$, and mixed-valent $\mathbf{5}^{3-}$, could be studied by single-crystal X-ray diffraction. This provides unprecedented structural information and reveals that the [2Fe−2S] core undergoes only minor structural changes upon protonation or reduction, which is in line with low reorganization energies upon PCET. However, subtle variations of the [2Fe−2S] core in the diferric $\mathbf{5}^{2-}$ and mixed-valent $\mathbf{5}^{3-}$ states reflect that the additional electron is largely localized at the N-coordinated Fe site, in accordance with EPR and Mössbauer evidence. It is somewhat surprising and counterintuitive though that the more pronounced valence localization caused by the heteroleptic $\{N_2/S_2\}$ ligation does not lead to larger core structural changes compared to homoleptically coordinated [2Fe−2S] complexes.

The thermodynamics of the PCET square scheme have been fully elucidated. Both the difference in p$K_a$ for diferric $\mathbf{5H}^{-}$ and mixed-valent $\mathbf{5H}^{2-}$ of about 4 units and the anodic shift of the reduction potential of around +230 mV upon protonation are in very good agreement with data for the biological system. The BDFE of the N−H bond of the protonated cluster $\mathbf{5H}^{2-}$ (60.2 ± 0.5 kcal mol$^{-1}$) is around 10−15 kcal mol$^{-1}$ lower than values reported for biological Rieske clusters, but similar to the N−H BDFE for a recently reported homoleptic [2Fe−2S] cluster. However, despite these similar BDFEs (and hence similar free energies $\Delta G^{\circ}_{CPET}$), the reaction of the protonated mixed-valent cluster with TEMPO, yielding TEMPO-H and the nonprotonated diferric cluster, is significantly faster for the present system $\mathbf{5H}^{2-}$ compared to the homoleptic complexes. While steric factors cannot be excluded at this point, it is an interesting perspective that this might be an effect of increased localization of electron density at the PCET site in $\mathbf{5H}^{2-}$, which would suggest some further rationale for nature's choice of the Rieske-type [2Fe−2S] core with its heteroleptic $\{N_2/S_2\}$ ligation.

The present new model system is only the second synthetic analogue emulating the heteroleptic ligation of the Rieske cofactor,[11] and the first that features a biomimetic $\{His_2Cys_2\}$-like ligation amenable to PCET at the N-coordinated subsite of the [2Fe−2S] cluster. It thus represents an excellent structural, spectroscopic, and functional analogue, and it is the highest fidelity Rieske model known so far.

## ASSOCIATED CONTENT

### Supporting Information

Synthetic procedures, complete experimental details, $^1$H NMR and UV−vis titration, additional EPR and Mössbauer spectra, details of the kinetic investigations, and crystallographic details (CIF) for $(CoCp^*_2)_2\mathbf{5}$, $(NEt_4)_3\mathbf{5}$·DMF, and $(NEt_4)\mathbf{5H}$·2DMF·$Et_2O$. This material is available free of charge via the Internet at http://pubs.acs.org.

## AUTHOR INFORMATION


### Corresponding Author

franc.meyer@chemie.uni-goettingen.de

### Present Address

[§]C.T.S.: Department of Chemistry, University of Utah, 315 S. 1400 East, Salt Lake City, UT 84112.


### Notes

The authors declare no competing financial interest.

## ACKNOWLEDGMENTS

We thank Dr. Eberhard Bothe and Dr. Eckhard Bill (Max Planck Institute for Chemical Energy Conversion, Mülheim, Germany) for CPC and EPR measurements. Financial support by the DFG (International Research Training Group GRK 1422 "Metal Sites in Biomolecules: Structures, Regulation and Mechanisms"; see www.biometals.eu) and the Cusanuswerk (Ph.D. fellowship for A.A.) is gratefully acknowledged. C.T.S. (Grant GM099316) and J.M.M. (Grant GM50422) gratefully acknowledge the U.S. National Institutes of Health.

## REFERENCES


(1) (a) Rieske, J. S.; MacLennan, D. H.; Coleman, R. *Biochem. Biophys. Res. Commun.* **1964**, *15*, 338. (b) Rieske, J. S. *J. Biol. Chem.* **1968**, *239*, 3017.

(2) (a) Link, T. A. *Adv. Inorg. Chem.* **1999**, *47*, 83. (b) Ferraro, D. J.; Gakhar, L.; Ramaswamy, S. *Biochem. Biophys. Res. Commun.* **2005**, *338*, 175.

(3) Crofts, A. R. *Biochim. Biophys. Acta, Bioenerg.* **2004**, *1655*, 77.

(4) Link, T. A. *FEBS Lett.* **1997**, *412*, 257.

(5) (a) Kuila, D.; Fee, J. A. *J. Biol. Chem.* **1986**, *261*, 2768. (b) Nitschke, W.; Joliot, P.; Liebl, U.; Rutherford, A. W.; Hauska, G.; Müller, A.; Riedel, A. *Biochim. Biophys. Acta, Bioenerg.* **1992**, *1102*, 266. (d) Zu, Y.; Fee, J. A.; Hirst, J. *J. Am. Chem. Soc.* **2001**, *123*, 9906. (e) Zu, Y.; Couture, M. M. J.; Kolling, D. R. J.; Crofts, A. R.; Eltis, L. D.; Fee, J. A.; Hirst, J. *Biochemistry* **2003**, *42*, 12400.

(6) (a) Lin, I. J.; Chen, Y.; Fee, J. A.; Song, J.; Westler, W. M.; Markley, J. L. *J. Am. Chem. Soc.* **2006**, *128*, 10672. (b) Hsueh, K.-L.; Westler, W. M.; Markley, J. L. *J. Am. Chem. Soc.* **2010**, *132*, 7908.

(7) Lhee, S.; Kolling, D. R. J.; Nair, S. K.; Dikanov, S. A.; Crofts, A. R. *J. Biol. Chem.* **2010**, *285*, 9233.

(8) Cape, J. L.; Bowman, M. K.; Kreamer, D. M. *J. Am. Chem. Soc.* **2005**, *127*, 4208.

(9) Kramer, D. M.; Nitschke, W.; Cooley, J. W. *Adv. Photosynth. Respir.* **2009**, *28*, 451.

(10) Rao, P. V.; Holm, R. H. *Chem. Rev.* **2004**, *104*, 527.

(11) Ballmann, J.; Albers, A.; Demeshko, S.; Dechert, S.; Bill, E.; Bothe, E.; Ryde, U.; Meyer, F. *Angew. Chem. Int. Ed.* **2008**, *47*, 9537.

(12) (a) Salifoglou, A.; Simopoulos, A.; Kostikas, A.; Dunham, W. R.; Kanatzidis, M. G.; Coucouvanis, D. *Inorg. Chem.* **1988**, *27*, 3394. (b) Cleland, W. E.; Averill. *Inorg. Chem.* **1984**, *23*, 4192. (c) Beardwood, P.; Gibson, J. F. *J. Chem. Soc., Chem. Commun.* **1986**, 490.

(13) Albers, A.; Demeshko, S.; Dechert, S.; Bill, E.; Bothe, E.; Meyer, F. *Angew. Chem., Int. Ed.* **2011**, *50*, 9191.

(14) Saouma, C. T.; Kaminsky, W.; Mayer, J. M. *J. Am. Chem. Soc.* **2012**, *134*, 7293.

(15) Albers, A.; Bayer, T.; Demeshko, S.; Dechert, S.; Meyer, F. *Chem.—Eur. J.* **2013**, *19*, 10101.

(16) Albers, A.; Demeshko, S.; Pröpper, K.; Dechert, S.; Bill, E.; Meyer, F. *J. Am. Chem. Soc.* **2013**, *135*, 1704.

(17) Bönisch, H.; Schmidt, C. L.; Schäfer, G.; Ladenstein, R. *J. Mol. Biol.* **2002**, *319*, 791.

(18) Iwata, S.; Saynovits, M.; Link, T. A.; Michel, H. *Structure* **1996**, *4*, 567.

(19) Carrell, C. J.; Zhang, H.; Cramer, W. A.; Smith, J. L. *Structure* **1997**, *5*, 1613.

(20) Akalay, D.; Dürner, G.; Bats, J. W.; Bolte, M.; Göbel, M. W. *J. Org. Chem.* **2007**, *72*, 5618.

(21) Kaljurand, I.; Kütt, A.; Sooväli, L.; Rodima, T.; Mäemets, V.; Leito, I.; Koppel, I. A. *J. Org. Chem.* **2005**, *70*, 1019.

(22) Bertrand, P.; Guigliarelli, B.; Gayda, J. P.; Beardwood, P.; Gibson, J. F. *Biochim. Biophys. Acta, Protein Struct. Mol. Enzymol.* **1985**, *831*, 261.
(23) (a) Link, T. A. In *Handbook of Metalloproteins*; Messerschmidt, A., Huber, R., Wieghardt, K., Poulos, T., Eds.; John Wiley & Sons: Chichester, U.K., 2001; Vol. *1*, p 518. (b) Boxhammer, S.; Glaser, S.; Kühl, A.; Wagner, A. K.; Schmidt, C. L. *Biometals* **2008**, *21*, 459.
(24) Orio, M.; Mouesca, J. M. *Inorg. Chem.* **2008**, *47*, 5394.
(25) Fee, J. A.; Findling, K. L.; Yoshida, T.; Hille, R.; Tarr, G. E.; Hearshen, D. O.; Dunham, W. R.; Day, E. P.; Kent, T. A.; Münck, E. *J. Biol. Chem.* **1984**, *259*, 124.
(26) Bowman, M. K.; Berry, E. A.; Roberts, A. G.; Kramer, D. M. *Biochemistry* **2004**, *43*, 430.
(27) Riedel, A.; Rutherford, A. W.; Hauska, G.; Müller, A.; Nitschke, W. *J. Biol. Chem.* **1991**, *266*, 17838.
(28) Hoggins, J. T.; Steinfink, H. *Inorg. Chem.* **1976**, *15*, 1682. Mössbauer data at 300 K have been used for establishing the correlation.
(29) Schünemann, V.; Trautwein, A. X.; Illerhaus, J.; Haehnel, W. *Biochemistry* **1999**, *38*, 8981.
(30) Pikus, J. D.; Studts, J. M.; Achim, C.; Kauffmann, K. E.; Münck, E.; Steffan, R. J.; McClay, K.; Fox, B. G. *Biochemistry* **1996**, *35*, 9106.
(31) Zu, Y.; Couture, M. M.; Kolling, D. R.; Crofts, A. R.; Eltis, L. D.; Fee, J. A.; Hirst, J. *Biochemistry* **2003**, *42*, 12400.
(32) (a) Klingen, A. R.; Ullmann, G. M. *Biochemistry* **2004**, *43*, 12383. (b) Kolling, D. J.; Brunzelle, J. S.; Lhee, S.; Crofts, A. R.; Nair, S. K. *Structure* **2007**, *15*, 29. (c) Brown, E. N.; Friemann, R.; Karlsson, A.; Parales, J. V.; Couture, M. M.-J.; Eltis, L. D.; Ramaswamy, S. *J. Biol. Inorg. Chem.* **2008**, *13*, 1301. (d) Iwasaki, T.; Fukuzawa, R.; Miyajima-Nakano, Y.; Baldansuren, A.; Matsushita, S.; Lin, M. T.; Gennis, R. B.; Hasegawa, K.; Kumasaka, T.; Dikanov, S. A. *J. Am. Chem. Soc.* **2012**, *134*, 19731.
(33) Warren, J. J.; Tronic, T. A.; Mayer, J. M. *Chem. Rev.* **2010**, *110*, 6961.
(34) Roth, J. P.; Yoder, J. C.; Won, T.-J.; Mayer, J. M. *Science* **2001**, *294*, 2524.
(35) Mader, E. A.; Larsen, A. S.; Mayer, J. M. *J. Am. Chem. Soc.* **2004**, *126*, 8066.